Journal of Saudi Chemical Society (2017) **21**, 878–886

King Saud University

Journal of Saudi Chemical Society

www.ksu.edu.sa
www.sciencedirect.com

ORIGINAL ARTICLE

Ytterbia doped nickel–manganese mixed oxide catalysts for liquid phase oxidation of benzyl alcohol

S.S.P. Sultana [a], Roushown Ali [b], Mufsir Kuniyil [a,c], Mujeeb Khan [c], Abdulrahman Alwarthan [c], D.H.V. Kishore [a], M.E. Assal [c], K.R.S. Prasad [a], Naushad Ahmad [c], Mohammed Rafiq H. Siddiqui [c], Syed F. Adil [c,*]

[a] *Department of Chemistry, K L University, Guntur, Andhra Pradesh 522502, India*
[b] *Department of Chemistry, University of Rajshahi, Rajshahi 6205, Bangladesh*
[c] *Department of Chemistry, College of Science, King Saud University, P.O. 2455, Riyadh 11451, Saudi Arabia*

Received 28 April 2017; revised 27 June 2017; accepted 8 July 2017
Available online 17 July 2017

KEYWORDS

Ytterbia;
Nickel–manganese mixed oxides;
Catalytic activity;
Oxidation;
Benzyl alcohol

Abstract Nickel–manganese mixed oxides doped with 1, 3, 5 mol% ytterbia have been prepared by co-precipitation method and used in the catalytic oxidation of benzyl alcohol. Catalytic activity of these oxides calcined at 400 °C and 500 °C was studied for selective oxidation of benzyl alcohol to the corresponding aldehyde using molecular oxygen as an oxidizing agent. The results showed that thermally stable 5 mol% ytterbia doped nickel–manganese oxide [Yb_2O_3-(5%)-Ni_6MnO_8] exhibited highest catalytic performance when it was calcined at 400 °C. A 100% conversion of the benzyl alcohol was achieved with >99% selectivity to benzaldehyde within a reaction period of 5 h at 100 °C. The mixed oxide prepared has been characterized by scanning election microscopy (SEM) and energy dispersive X-ray analysis (EDXA), X-ray diffraction (XRD), Fourier transform infrared spectroscopy (FT-IR), thermogravimetric analysis (TGA), Brunauer–Emmett–Teller (BET) and temperature programed reduction (H_2-TPR).

1. Introduction

Catalytic oxidation of alcohols plays a crucial role in the current chemical industry for the production of key intermediates such as aldehydes, epoxides, ketones and organic acids [1,2]. Developing practical and sustainable catalytic methods for selective oxidation reactions is an important challenge. The oxidation of alcohols to carbonyl compounds is fundamentally pivotal in life science and extremely useful for the preparation of many drugs from the view point of laboratory synthesis and

* Corresponding author.
E-mail address: sfadil@ksu.edu.sa (S.F. Adil).
Peer review under responsibility of King Saud University.

Production and hosting by Elsevier

http://dx.doi.org/10.1016/j.jscs.2017.07.002

industrial manufacturing [3,4]. In fact, some well-known highly difficult chemical reactions involve selective oxidation reactions such as selective oxidation of methane by molecular oxygen [5]. On the other hand, some aerobic oxidation of alcohols to the corresponding aldehydes is carried out in the liquid phase [6].

A variety of transition metals and noble metal oxide-based catalysts have been reported as solid catalysts for the catalytic oxidation of alcohols. However, the high cost and limited accessibility of the noble metals restrict their applications, while the mixed metal oxides were found to be very efficient due to their excellent catalytic activities for such reactions [7–11] among these the nickel–manganese based catalysts have been widely used because of their high activity and low cost [12–14]. It has also been extensively reported that the catalytic activity of mixed metal oxide enhanced significantly upon doping with nanoparticles of other elements [15,16].

Different elements have been used as dopants, among all, rare earth elements were used as excellent promoters due to their promising applications in various fields [17,18]. Specially ytterbium doped compounds have been reported as effective material in Ni–MH battery applications [19]. High power fiber lasers have some unique advantages including high conversion efficiency, excellent beam quality, small volume and weight. They are widely used in medical, military, industrial processing and modern telecommunication, which are based on double-clad fiber. As we know Yb^{3+} ions have two simple energy levels, and the upper energy level has long fluorescence life. They also have high quantum efficiency and wide absorption spectrum and are more frequently employed because of its high power and high efficient diode pumps with wave length of 900–1000 nm. Besides, Yb^{3+} ion has some advantages in comparison with other ions like Nd^{3+} [20,21]. These ytterbium doped materials are also used in glasses, as host materials for efficient energy storage [22]. Adjustable double clad ytterbium-doped fiber laser using a double-pass Mach–Zehnder interferometer used as a tunable filter and new ytterbium double-clad fiber lasers (DCFLs) were widely used due to their high efficiency, low cost and excellent beam quality. A mono mode ytterbium-doped nano sized titanium fiber laser has been used in various applications, such as photo catalysis, photo electric conversions and gas sensors [23,24].

Apart from the above mentioned uses of ytterbium, there are a plethora of examples wherein the oxides of ytterbium have been used as catalysts for many organic conversions, such as Machida et al. reportedly employed a catalyst comprising ytterbia for the oxidative coupling of methane, which was found to be stable up to 1000 °C and also for CO oxidation [25,26]. Ytterbia-stabilized zirconia was reported to possess higher oxygen exchange and diffusion, which has been used in the SOFCs [27].

In our previous work, we reported synthesis of nano ceria-doped nickel–manganese mixed oxide nano-catalysts and their application for the catalytic oxidation of benzyl alcohol as a model reaction [12]. In continuation of our previous work, the present manuscript deals with nano-structured ytterbia doped nickel–manganese oxide and its evaluation for oxidation of benzyl alcohol to benzaldehyde.

2. Experimental

2.1. Materials and methods

$Ni(NO_3)_2{\cdot}6H_2O$ (nickel nitrate), $Mn(NO_3)_2{\cdot}4H_2O$ (manganese nitrate), $Yb(NO_3)_3{\cdot}5H_2O$ (ytterbium nitrate), $NaHCO_3$ (sodium bicarbonate), $C_6H_5CH_2OH$ (benzyl alcohol), C_6H_5-CHO (benzaldehyde) and $C_6H_5CH_3$ (toluene) [Merck grade] were purchased from Sigma–Aldrich Pure Chemical Industries

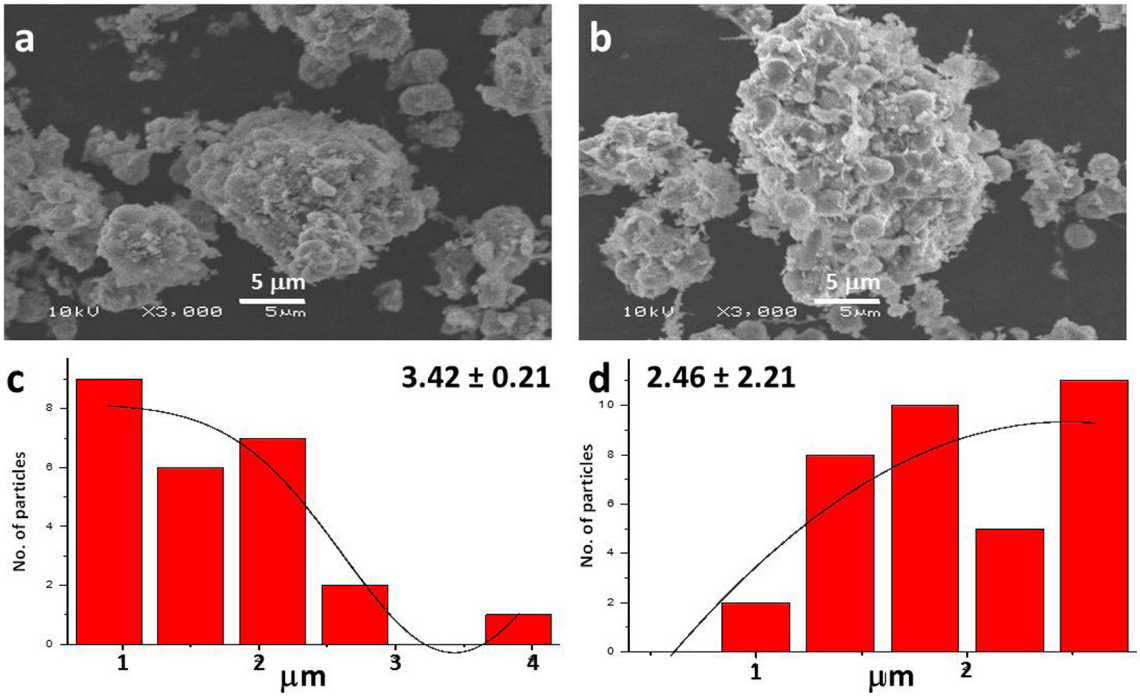

Fig. 1 SEM micrographs of Yb_2O_3-(5%)-Ni_6MnO_8 calcined at (a) 400 °C and (b) 500 °C and particle distribution graph of the catalysts Yb_2O_3-(5%)-Ni_6MnO_8 calcined at (c) 400 °C and (d) 500 °C.

Co., Ltd. They were used as received without further purification.

Structural morphology and elemental analysis was determined by JEOL JSM-6360A (Japan), scanning electron microscopy (SEM) attached with energy dispersive X-ray analysis (EDAX). Powder X-ray diffraction data were collected using a D2 phaser (Bruker) X-ray diffractometer. The infrared spectra were recorded using Perkin-Elmer 1000 (USA) FT-IR spectrophotometer in the region of 4000–500 cm^{-1}. Thermogravimetric analysis (TGA) was carried out using Perkin-Elmer Thermogravimetric Analyzer 7. The surface area of the oxides was obtained using Brunauer–Emmet–Teller (BET), measured on a NOVA 4200e surface area & pore size analyzer. Specific areas were calculated using the BET method from the nitrogen adsorption isotherms, recorded at the temperature of liquid nitrogen on a NOVA 4200e surface area & pore size analyzer, taking a value of 0.162 nm^2 for the cross-sectional area of the N_2 molecule adsorbed at 77 K. Temperature programed reduction (H_2-TPR) studies of active catalyst was performed on a chemisorption apparatus (Micromeritics AutoChem II-2920) equipped with a thermal conductivity detector using a mixture of 10% H_2/Ar at a flow rate of 20 mL min^{-1}. The temperature was ramped from room temperature to 500 °C at the heating rate of 10 °C/min. Water formed during the reduction was trapped by cold trap. After the run, TCD signal was plotted as a function of temperature.

2.2. Catalyst preparation

In a typical procedure to synthesize nickel–manganese oxides doped with 1, 3, 5 mol% ytterbia, stoichiometric volume of 0.2 M solution of nickel nitrate and manganese nitrate was mixed in a round bottomed flask. To this volume of 0.2 M solution, desired mol% of ytterbium nitrate solution was added. The resulting solution was heated to 90 °C, while stirring using a mechanical stirrer. To this solution, 1 M solution of $NaHCO_3$ was added drop wise until the solution attained a pH of 9. The solution was continued to stir at the same temperature for about 3 h and then it was left over night at room temperature while stirring. The solution was filtered using a Buchner funnel under vacuum and kept at 70 °C overnight. The dried products were then calcined at 400 °C and 500 °C.

2.3. Catalyst testing

In a typical reaction run, 150 mg of catalyst was loaded in a glass flask pre-charged with 0.2 mL (2 mmol) benzyl alcohol in 8 mL toluene. The mixture was then heated to 100 °C with vigorous stirring. Oxygen was bubbled at a flow rate of 20 mL min^{-1} to the mixture once the desired reaction temperature was attained. After reaction, the solid catalyst was separated by centrifugation and the conversion of the liquid samples was evaluated by gas chromatography (GC, 7890A), Agilent Technologies Inc., equipped with a flame ionization detector (FID) and a 19019S-001 HP-PONA capillary column.

3. Results and discussion

3.1. Catalyst characterization

3.1.1. Scanning electron microscopy (SEM)

The SEM images of Yb_2O_3-(5%)-Ni_6MnO_8 pre-calcined at 400 °C and 500 °C are shown in Fig. 1. The micrographs of the synthesized catalyst show no well-defined morphology. The surface of micrographs is not uniform and show size and morphology differences upon calcination. During the calcination process of reacting precursors, there were large amounts of small gaseous molecules emitted, which led to formation of pores in sample. A particle size distribution of the SEM images was calculated using the program Image J (Fig. 1(c–d)), and found to be equal to 3.42 and 2.46 μm for the catalyst calcined at 400, and 500 °C respectively.

3.1.2. X-ray diffraction (XRD) analysis

The XRD pattern of the Yb_2O_3-(5%)-Ni_6MnO_8 catalysts pre-calcined at 400 °C and 500 °C is shown in Fig. 2.

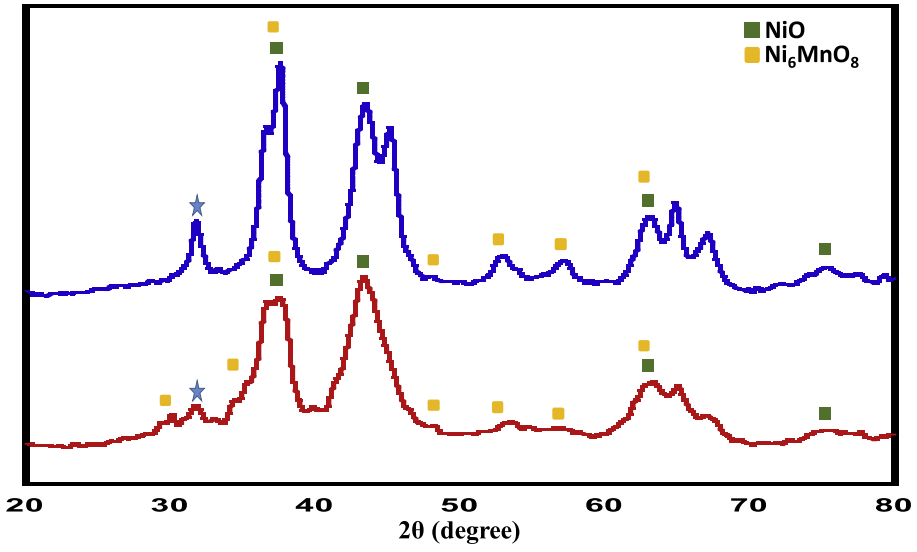

Fig. 2 XRD pattern of Yb_2O_3-(5%)-Ni_6MnO_8 pre-calcined at (a) 400 °C and (b) 500 °C. The reflections marked with asterisk (*) could be attributed to the presence of cubic phase of Yb_2O_3.

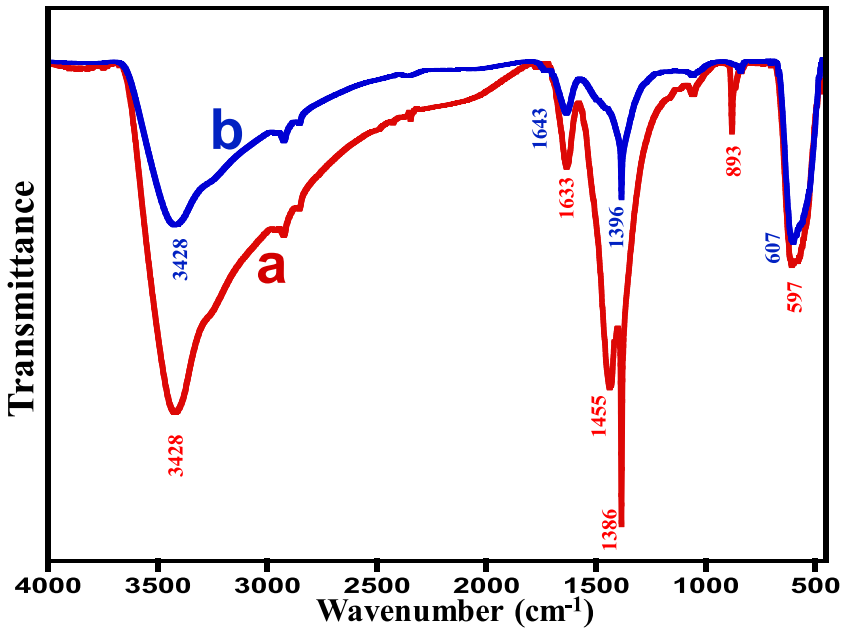

Fig. 3 FT-IR spectrums of Yb_2O_3-(5%)-Ni_6MnO_8 catalyst calcined at (a) 400 °C and (b) 500 °C.

The X-ray diffraction patterns of Yb_2O_3-(X%)-Ni_6MnO_8 are expected to be a mixture of two or more phases. However, upon analysis of the data obtained it was revealed that it was a mixture of Ni_6MnO_8 (JCPDS No.: 00-049-1295) and traces of NiO. The catalyst calcined at 400 °C is found to contain a mixture of Ni_6MnO_8 and traces of NiO, while the catalyst calcined at 500 °C was found to possess the mixture of Ni_6MnO_8 and traces of NiO along with some unidentified phases which happen to occur upon increase in calcination temperature from 400 °C to 500 °C, which could not be identified because of the limitation of reference data. To identify the mixture of the phases X-ray diffraction data with higher resolution having high intensity will be required. The crystallite size of the Yb_2O_3-(X%)-Ni_6MnO_8 was determined by the Scherrer equation using XRD line broadening. The crystallite size obtained was approximately 16 nm.

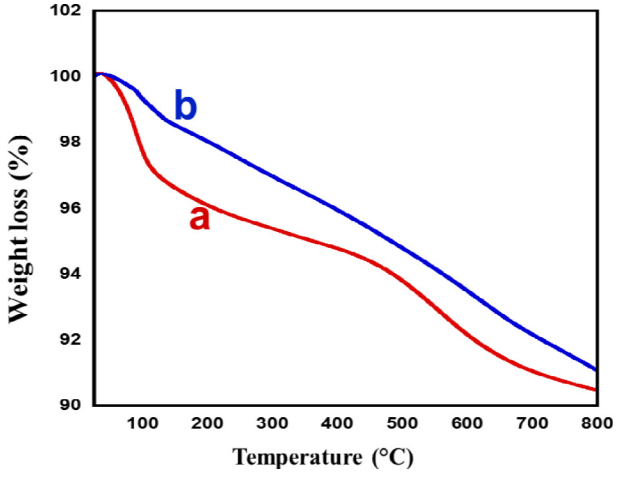

Fig. 4 Thermal stability pattern of the Yb_2O_3-(5%)-Ni_6MnO_8 catalyst pre-calcined at (a) 400 °C and (b) 500 °C.

3.1.3. FT-IR analysis

The Yb_2O_3-(5%)-Ni_6MnO_8 catalysts calcined at 400 °C and 500 °C were subjected to FT-IR spectroscopy and the spectra obtained are shown in Fig. 3. The peaks in the region 3450–3500 cm^{-1} correspond to the stretching vibrations of the OH group. The characteristic bands of νOH, located at 3450 cm^{-1} were found to be present in both catalysts. As the calcination temperature increases the intensity of these bands decreases which represents the decrease of hydroxyl group at higher temperature. The peaks in the region of 1600-1500 cm^{-1} can be attributed to νOH bending vibrations. Intense peaks are noticed in the range of 525–615 cm^{-1} which are characteristic of various oxides of manganese.

Table 1 Weight loss of (1, 3 and 5 mol%) Yb_2O_3-Ni_6MnO_8 catalysts.

Composition	Calcination Temperature	
	400 °C	500 °C
Yb_2O_3-(1%)-Ni_6MnO_8	17%	16%
Yb_2O_3-(3%)-Ni_6MnO_8	15%	13%
Yb_2O_3-(5%)-Ni_6MnO_8	8%	9%

Table 2 Textural properties of the synthesized catalysts.

Calcination temperature	$S_{(BET)}$ (m^2/g)[a]	$V_{(Pore)}$ (cm^3/g)[b]	$D_{(Pore)}$ (A°)[c]
400 °C	41.5	0.016	18.5
500 °C	55.1	0.022	18.6

[a] Specific surface area $S_{(BET)}$ calculated by BET equation.
[b] Total pore volume estimated at P/Po = 0.99.
[c] Pore diameter calculated by BJH method.

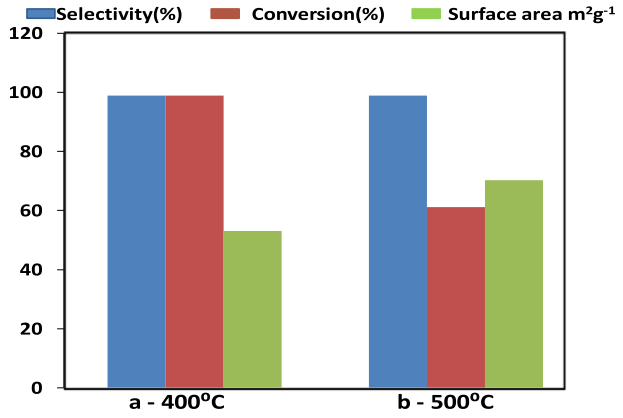

Fig. 5 BET of Yb_2O_3-(5%)-Ni_6MnO_8 catalyst pre-calcined at (a) 400 °C and (b) 500 °C.

3.1.4. TGA analysis

The thermal stability of the Yb_2O_3-(5%)- Ni_6MnO_8 catalyst calcined at 400 °C and 500 °C were studied using TGA analysis. The thermogram of the synthesized catalyst is shown in Fig. 4. The percentage of weight lost during the thermogravimetric analysis of the synthesized catalyst is presented in Table 1. The weight loss of the 1%, 3% and 5% Yb_2O_3 doped oxides calcined at 400 °C shows similar trend with that at 500 °C. The TGA analysis of these catalysts revealed that the weight loss of the catalyst decreases with the increasing percentage of doping. Therefore, the catalyst Yb_2O_3-(5%)- Ni_6MnO_8 is thermally most stable compared to the other compositions. From the TGA pattern obtained for the catalyst Yb_2O_3-(5%)-Ni_6MnO_8 calcined at 400 °C and 500 °C (Fig. 4), it can be observed that there is a weight loss of about 3% when the sample is heated up to 100 °C, which can be attributed to the loss of water molecules in the form of moisture in the catalyst Yb_2O_3-(5%)-Ni_6MnO_8 calcined at 400 °C and the same pattern of weight loss is observed in the case of the catalyst calcined at 500 °C. However, in case of the catalyst Yb_2O_3-(5%)-Ni_6MnO_8 calcined at 400 °C, upon further increase in temperature it was found that in the temperature range of 400–600 there is an additional weight loss of 3%, which can be attributed to the phase formation/changes taking place at this temperature range.

3.1.5. BET analysis

The BET surface area analysis shows Yb_2O_3-(5%)-Ni_6MnO_8 calcined at 400 °C has slightly lower surface area compared with that calcined at 500 °C. The calcination temperature shows an effect on the surface area, although there was a very subtle change in pore size, while no change was observed in the pore diameter. The values obtained are given in Table 2 (Fig. 5).

3.1.6. Temperature programed reduction of catalysts (H_2-TPR)

Temperature-programed reduction (H_2-TPR) profiles of Yb_2O_3-(5%)-Ni_6MnO_8 pre-calcined at 400 °C and 500 °C are shown in Fig. 6. TPR patterns of catalysts are different, both in broadness and intensity. The difference in TPR pattern revealed that calcination temperature has a definite effect on the reduction behavior of catalysts. Two H_2-consumption peaks were observed in pattern: the low intensity peak at 290 °C and the high intense peak at 335 °C for the catalyst calcined at 400 °C. For this catalyst the first peak is attributed to reduction of bulk NiO while second high intensity peak is assigned to reduction of Ni-Mn species. As the temperature is increased to 500 °C it was observed that positive shift of the high intense peak at 375 °C and peak became broader for this sample. This is probably due to the combined reduction of the intermediate known phase (Ni_6MnO_8 and NiO) and undefined phase, confirmed by XRD. In fact, the positive shift in temperature is due to increase in metal-support interaction which in turn leads to higher surface area of the catalyst.

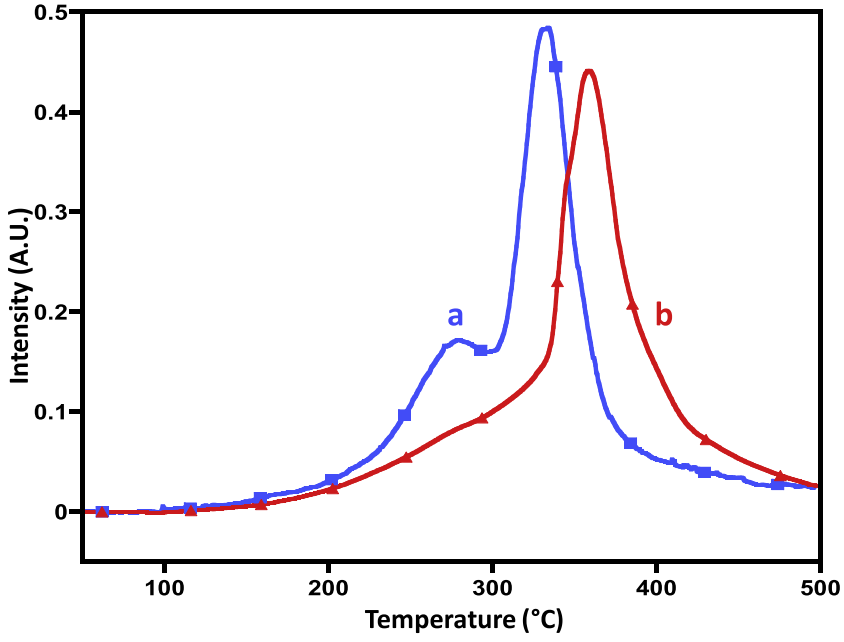

Fig. 6 TPR of Yb_2O_3-(5%)-Ni_6MnO_8 catalyst pre-calcined at (a) 400 °C and (b) 500 °C.

3.1.7. Catalytic evaluation

To ascertain the catalytic performance of synthesized oxides, oxidation of benzyl alcohol to the corresponding aldehyde was carried out using molecular oxygen as an oxidizing agent. The mol% percentage of ytterbia doped and calcination temperature were varied in order to confirm the optimum percentage of ytterbia required and the appropriate calcination temperature for the best catalytic conversion by the synthesized catalyst. The reaction was carried out for 5 h and results obtained are as mentioned below.

When the catalyst Yb_2O_3-(1%)-Ni_6MnO_8 pre-calcined at 400 °C and 500 °C was subjected to oxidation of benzyl alcohol to benzaldehyde, the catalyst calcined at 400 °C yielded 85% conversion to product, while the catalyst calcined at 500 °C gave only 37% conversion to benzaldehyde. Similarly, the catalyst Yb_2O_3-(3%)-Ni_6MnO_8 calcined at 400 °C and 500 °C showed 94% and 35% conversion to benzaldehyde, respectively. When the catalyst Yb_2O_3-(5%)-Ni_6MnO_8 calcined at 400 °C was employed, it was found that the catalyst yielded ~ 60% conversion within first 60 min and on continuation a 100% conversion of benzyl alcohol to benzaldehyde was obtained after 240 min. On the other hand, the same catalyst pre-calcined at 500 °C yielded 61% conversion. The graphical illustration of kinetics for the conversion reaction is given in Fig. 7. It has been reported that the benzaldehyde obtained from oxidation of benzyl alcohol usually undergoes further oxidation to benzoic acid, however in our experiments no further oxidation takes place, hence it can be concluded that the catalysts yielded >99% selectivity. Furthermore, it has also been observed that the catalyst does not oxidize the solvent used, i.e., toluene, while forming the conversion product, i.e., benzaldehyde.

From the results obtained it can be observed that the catalyst Yb_2O_3-(5%)-Ni_6MnO_8 calcined at 400 °C exhibits higher conversion (Fig. 5) compared with that calcined at 500 °C, however the BET surface analysis of the sample revealed that the catalyst calcined at 400 °C has a surface area of 41 m^2/g while the catalyst calcined at 500 °C has a surface area of 55 m^2/g. This shows that the surface area is not the only factor that is playing an important role in the catalytic performance of the prepared catalysts but also the phase composition. From the XRD analysis it was found that the prepared catalyst possesses a mixture of Ni_6MnO_8 and traces of NiO when calcined at 400 °C, however upon calcination at higher temperature, i.e., 500 °C, there is a formation of another unidentified phase along with the Ni_6MnO_8 and traces of NiO. Hence it can be assumed that the formation of new unidentified phase in the catalyst calcined at 500 °C may be restricting the access of the active site of the catalyst which could be responsible for the decrease in the catalytic performance of the catalyst.

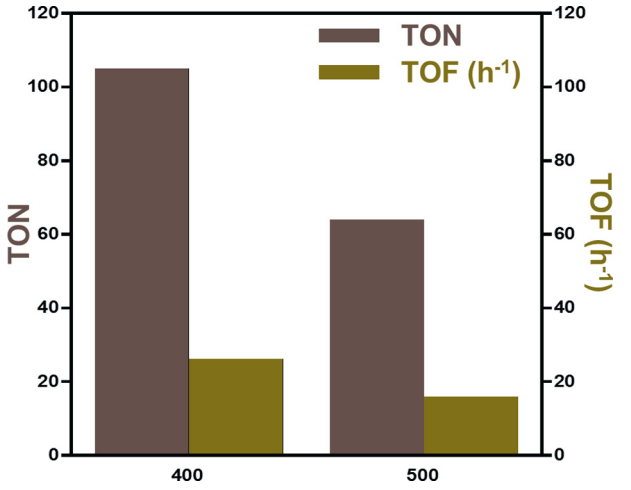

Fig. 8 Graphical representation TOF and TON for the catalyst: Yb_2O_3-(5%)-Ni_6MnO_8 catalyst calcined at (a) 400 °C; (b) and 500 °C.

The catalytic performance of the prepared catalyst was compared employing Turnover Number (TON) and Turnover Frequency (TOF). The Turnover Number (TON) of the prepared catalyst Yb_2O_3-(5%)-Ni_6MnO_8 calcined at 400 °C and 500 °C was calculated and it was found to be 105.0 and 64.09 respectively, while Turnover Frequency (TOF) was found to be 26.27 h^{-1} for the catalyst Yb_2O_3-(5%)-Ni_6MnO_8 calcined at 400 °C, while for the catalyst calcined at 500 °C was 16.02 h^{-1}. A graphical representation of the values obtained is given in Fig. 8. Further a comparison of the specific activity of the best catalyst was made between the NiMnO mixed oxides with various dopants and it was found that the catalyst Yb_2O_3-(5%)-Ni_6MnO_8 calcined at 400 °C is better than most of the catalyst reported earlier. A pictorial illustration of the comparison made is given in Fig. 9.

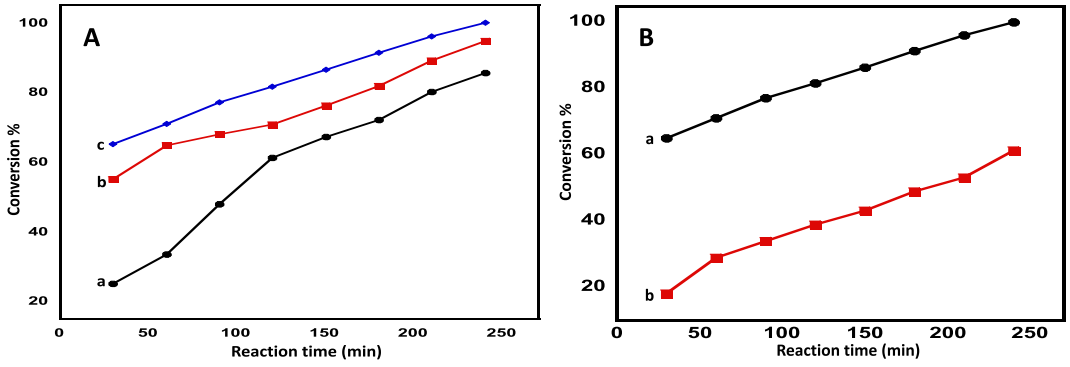

Fig. 7 Graphical representation of conversion (%) vs reaction time using catalyst Yb_2O_3-(X%)-Ni_6MnO_8 [A] (a) 1 mol%, (b) 3 mol% and (c) 5 mol% ytterbia doped Ni_6MnO_8 pre-calcined at 400 °C [B] (a) catalyst Yb_2O_3-(5%)-Ni_6MnO_8 pre-calcined at 400 °C and (b) at 500 °C **Reaction conditions:** Catalyst 150 mg, Reaction temperature 100 °C; Oxygen flow rate 20 mL min^{-1}; Benzyl alcohol 2 mmol; Toluene 10 mL.

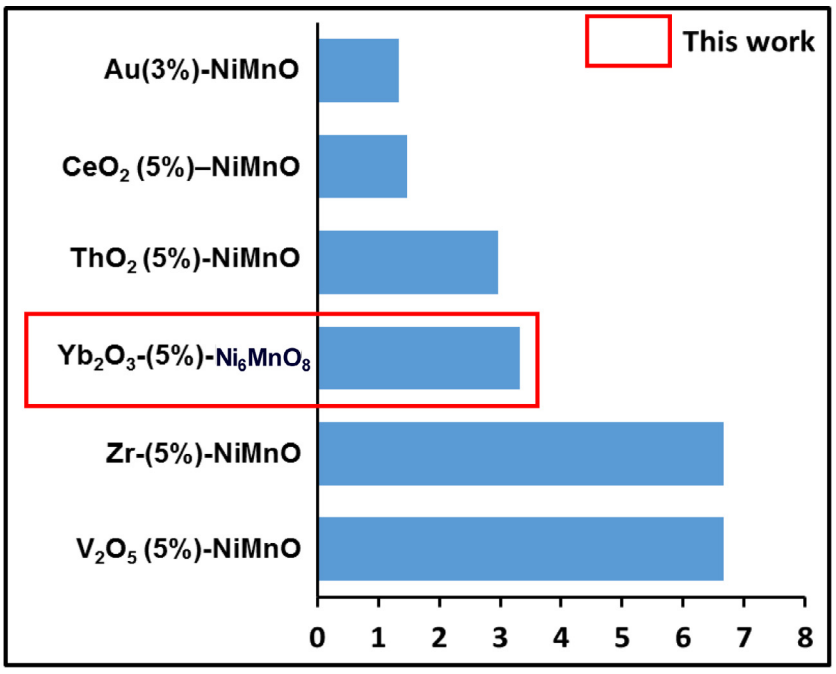

Fig. 9 A graphical representation of comparison of specific activity values obtained from our results and various NiMnO catalysts used for the oxidation of benzyl alcohol to benzaldehyde.

Table 3 A comparison between our result and earlier reported results in the literature for the oxidation of Benzyl alcohol to benzaldehyde.

Catalyst	Conv. (%)	Sel. (%)	Temp. (°C)	Sp. activity (mmol g^{-1} h^{-1})	Ref.
NbP-S2	43	65	90	9.81	[28]
Amorphous MnO_x	72	99	100	9.7	[29]
Au–Pd/MgO	< 52	100	80	9.43	[30]
Mn_6Ni_4	89	99	100	8.90	[31]
Mn_4Ni_6	73	99	100	7.4	[31]
Mn_8Ni_2	65	97	100	6.5	[31]
V_2O_5 (5%)-NiMnO	100	> 99	100	6.67	[32]
Zr (5%): NiMnO	100	> 99	100	6.67	[33]
Mn_2Ni_8	62	98	100	6.2	[31]
Ti-SBA-15	62	95	60	6.20	[34]
OMS-2	44	99	100	5.9	[29]
Au/RGO	65	93	100	5.42	[35]
KMn-i/CNTs	66.8	< 99	100	5.34	[36]
Mn_0Ni_{10}	51	98	100	5.20	[31]
ɣ-MnO_2	39	98	100	5.2	[29]
Ni–Cr hydrotalcite	11	98	100	4.1	[37]
MnOOH	66	99	100	4.1	[38]
CNTs-1	96.2	88.3	90	3.85	[39]
Yb_2O_3(5%)-Ni_6MnO_8	100	> 99	100	3.33	This work
1%Ag–MnO_2	100	< 99	100	3.33	[40]
$Ni(OH)_2$	98	98	100	3.3	[41]
Mn_3O_4-NiO-Ni/CNTs	32.9	< 99	100	3.29	[42]
ThO_2 (5%)-NiMnO	100	> 99	100	2.96	[43]
Ru/Mg–LaO	75	69	120	1.84	[44]
Ni–Fe hydrotalcite	4.6	98	100	1.7	[37]
CeO_2 (5%)–NiMnO	100	> 99	100	1.48	[12]
Au(3%)-NiMnO	100	> 99	100	1.33	[45]
Pd/AC	48.8	45.9	110	1.30	[46]
Au/CuO	85.7	< 99	80	1.29	[47]
$CoAl_2O_4$	90.98	86.95	80	1.14	[48]
$Mn_{10}NiO$	11	93	100	1.1	[31]
$Mg_{2.5}Ni_{0.5}$Al HT	52	97	100	0.4	[49]
Ni–Al hydrotalcite	31	99	100	0.1	[50]
MnO_x/MCM-41	94	99	80	0.026	[51]

Furthermore the specific activity of the best catalyst from the synthesized material was compared with the various other catalysts reported earlier for the same conversion of benzyl alcohol to benzaldehyde. It was found that the specific activity of the synthesized catalyst is less than various catalysts while it was found to be better than many other catalysts. The comparison list is compiled and given it Table 3.

4. Conclusion

We have synthesized Yb_2O_3-doped nickel–manganese oxide catalysts using facile co-precipitation method by varying the percentage of ytterbia-doping in the catalyst system. The prepared catalysts were calcined at 400 °C and 500 °C. Among different percentages of ytterbia-doped catalysts, 5 mol% Yb_2O_3-doped Ni_6MnO_8 pre-calcined at 400 °C gave 100% conversion of benzyl alcohol to benzaldehyde with >99% selectivity, which can be attributed to the formation of mixed phase of Ni_6MnO_8 and NiO. It can be concluded that calcination temperature plays a vital role in forming an active and durable catalyst. The synthesized catalyst exhibited high thermal stability and high catalytic activity for selective oxidation of benzyl alcohol to benzaldehyde using molecular oxygen as an oxidizing agent. Further studies into the application of the catalyst to various other alcohols needs to be tested and shall be reported in detail in a separate study.

Acknowledgements

The authors extend their appreciation to the Deanship of Scientific Research at King Saud University for funding this work through the research group project No. RG-1436-032.

References

[1] A. Rezaeifard, M. Jafarpour, A. Naeimi, A practical innovative method for highly selective oxidation of alcohols in neat water using water-insoluble iron and manganese porphyrins as reusable heterogeneous catalysts, Catal. Commun. 16 (1) (2011) 240–244.
[2] P.T.M. Pham, T.M. Le, I. Van Driessche, Co_3O_4 catalysts on CeO_2-ZrO_2 supports and Co_3O_4-CeO_2 catalysts on Al_2O_3/SiO_2 supports for the oxidation of propylene, J. Chem. 2015 (2015).
[3] R. Ali, K. Nour, A. Al-warthan, M.R.H. Siddiqui, Selective oxidation of benzylic alcohols using copper-manganese mixed oxide nanoparticles as catalyst, Arab. J. Chem. 8 (4) (2015) 512–517.
[4] Q. Cao, L.M. Dornan, L. Rogan, N.L. Hughes, M.J. Muldoon, Aerobic oxidation catalysis with stable radicals, Chem. Commun. 50 (35) (2014) 4524–4543.
[5] Z. Guo, B. Liu, Q. Zhang, W. Deng, Y. Wang, Y. Yang, Recent advances in heterogeneous selective oxidation catalysis for sustainable chemistry, Chem. Soc. Rev. 43 (10) (2014) 3480–3524.
[6] S.E. Davis, M.S. Ide, R.J. Davis, Selective oxidation of alcohols and aldehydes over supported metal nanoparticles, Green Chem. 15 (1) (2013) 17–45.
[7] I.E. Wachs, K. Routray, Catalysis science of bulk mixed oxides, ACS Catal. 2 (6) (2012) 1235–1246.
[8] M.B. Gawande, R.K. Pandey, R.V. Jayaram, Role of mixed metal oxides in catalysis science-versatile applications in organic synthesis, Catal. Sci. Tech. 2 (6) (2012) 1113–1125.
[9] P. Sarmah, R.K. Barman, P. Purkayastha, S.J. Bora, P. Phukan, B.K. Das, Copper (II) catalysed oxidation of alcohols in aqueous medium, Indian J. Chem., Sect A 48 (5) (2009) 637.
[10] X. Chu, C. Wang, L. Guo, Y. Chi, X. Gao, X. Yang, Mesoporous silica supported Au nanoparticles with controlled size as efficient heterogeneous catalyst for aerobic oxidation of alcohols, J. Chem. 2015 (2015).
[11] H.R. Rafiee, M. Feyzi, F. Jafari, B. Safari, Preparation and Characterization of Promoted Fe-V/SiO 2 Nanocatalysts for Oxidation of Alcohols, J. Chem. 2013 (2013).
[12] S. Sultana, D. Kishore, M. Kuniyil, M. Khan, A. Alwarthan, K. Prasad, J.P. Labis, S. Adil, Ceria doped mixed metal oxide nanoparticles as oxidation catalysts: Synthesis and their characterization, Arab. J. Chem. 8 (6) (2015) 766–770.
[13] S.F. Adil, S. Alabbad, M. Kuniyil, M. Khan, A. Alwarthan, N. Mohri, W. Tremel, M.N. Tahir, M.R.H. Siddiqui, Vanadia supported on nickel manganese oxide nanocatalysts for the catalytic oxidation of aromatic alcohols, Nanoscale Res. Lett. 10 (1) (2015) 1–9.
[14] M.H.-S. Ouaguenouni, A. Benadda, A. Kiennemann, A. Barama, Preparation and catalytic activity of nickel–manganese oxide catalysts in the reaction of partial oxidation of methane, Comptes Rendus Chimie 12 (6) (2009) 740–747.
[15] W.A.W.A. Bakar, R. Ali, N.S. Mohammad, The effect of noble metals on catalytic methanation reaction over supported Mn/Ni oxide based catalysts, Arab. J Chem (2013).
[16] C. Parmeggiani, F. Cardona, Transition metal based catalysts in the aerobic oxidation of alcohols, Green Chem. 14 (3) (2012) 547–564.
[17] J. Reszczyńska, T. Grzyb, J.W. Sobczak, W. Lisowski, M. Gazda, B. Ohtani, A. Zaleska, Visible light activity of rare earth metal doped (Er^{3+}, Yb^{3+} or Er^{3+}/Yb^{3+}) titania photocatalysts, Appl. Catal., B 163 (2015) 40–49.
[18] B. Diaz-Herrera, E. Jimenez-Rodriguez, B. Gonzalez-Diaz, A. Montesdeoca-Santana, J. Velazquez, R. Guerrero-Lemus, Combined up conversion, down conversion and down shifting photo-luminescence of low cost erbium–ytterbium Co-doped porous silicon produced by stain etching, Thin Solid Films 519 (18) (2011) 6110–6114.
[19] X.M. He, L. Wang, W. Li, C.Y. Jiang, C.R. Wan, Ytterbium coating of spherical $Ni(OH)_2$ cathode materials for Ni-MH batteries at elevated temperature, J. Power Sources 158 (2) (2006) 1480–1483.
[20] G. Hu, C. Shan, X. Deng, J. Zhang, Y. Pan, L. Wang, Threshold characteristics of linear cavity Yb^{3+}-doped double-clad fiber laser, Opt. Laser Technol. 37 (1) (2005) 3–7.
[21] M. Ivanov, Y. Kopylov, V. Kravchenko, L. Jiang, A. Medvedev, P. Yubai, Highly transparent ytterbium doped yttrium lanthanum oxide ceramics, J. Rare Earth 32 (3) (2014) 254–258.
[22] L. Courrol, L. Kassab, A. Morais, C. Mendes, L. Gomes, N. Wetter, N. Vieira, F. Cassanjes, Y. Messaddeq, S. Ribeiro, Study of the most suitable new glass laser to incorporate ytterbium: alkali niobium tellurite, lead fluorborate or heavy metal oxide, J. Lumin. 102 (2003) 106–111.
[23] Y. Meng, S. Zhang, X. Wang, J. Du, H. Li, Y. Hao, X. Li, Tunable double-clad ytterbium-doped fiber laser based on a double-pass Mach-Zehnder interferometer, Opt. Lasers Eng. 50 (3) (2012) 303–307.
[24] M. Boutinguiza, J. del Val, A. Riveiro, F. Lusquiños, F. Quintero, R. Comesaña, J. Pou, Synthesis of titanium oxide nanoparticles by Ytterbium fiber laser ablation, Phys. Procedia 41 (2013) 787–793.
[25] W.C. Mackrodt, M. Fowles, M.A. Morris, Oxidation catalysts. Google Patents: 1992.
[26] W.-P. Dow, T.-J. Huang, Yttria-stabilized zirconia supported copper oxide catalyst: II. Effect of oxygen vacancy of support on

catalytic activity for CO oxidation, J. Catal. 160 (2) (1996) 171–182.
[27] M. De Ridder, R. Van Welzenis, H. Brongersma, U. Kreissig, Oxygen exchange and diffusion in the near surface of pure and modified yttria-stabilised zirconia, Solid State Ion. 158 (1) (2003) 67–77.
[28] M.C. Reis, S.D. Barros, E.R. Lachter, R.A. San Gil, J.H. Flores, M.I.P. da Silva, T. Onfroy, Synthesis, characterization and catalytic activity of meso-niobium phosphate in the oxidation of benzyl alcohols, Catal. Today 192 (1) (2012) 117–122.
[29] H. Jing, K.Q. Sun, D.P. He, B.Q. Xu, Amorphous manganese oxide for catalytic aerobic oxidation of benzyl alcohol, Chin. J. Catal. 28 (12) (2007) 1025–1027.
[30] G. Zhan, Y. Hong, V.T. Mbah, J. Huang, A.-R. Ibrahim, M. Du, Q. Li, Bimetallic Au–Pd/MgO as efficient catalysts for aerobic oxidation of benzyl alcohol: A green bio-reducing preparation method, Appl. Catal., A 439 (2012) 179–186.
[31] Q. Tang, C. Wu, R. Qiao, Y. Chen, Y. Yang, Catalytic performances of Mn–Ni mixed hydroxide catalysts in liquid-phase benzyl alcohol oxidation using molecular oxygen, Appl. Catal., A 403 (1) (2011) 136–141.
[32] S.F. Adil, S. Alabbad, M. Kuniyil, M. Khan, A. Alwarthan, N. Mohri, W. Tremel, M.N. Tahir, M.R. Siddiqui, Vanadia supported on nickel manganese oxide nanocatalysts for the catalytic oxidation of aromatic alcohols, Nanoscale Res. Lett. 10 (1) (2015) 52.
[33] S. Alabbad, S.F. Adil, A. Alwarthan, M.R.H. Siddiqui, Liquid phase selective oxidation of aromatic alcohols employing nanoparticles of zirconia supported on nickel manganese oxide: synthesis, characterization and catalytic evaluation, Asian J. Chem. 25 (16) (2013) 8927–8932.
[34] R.V. Sharma, K.K. Soni, A.K. Dalai, Preparation, characterization and application of sulfated Ti-SBA-15 catalyst for oxidation of benzyl alcohol to benzaldehyde, Catal. Commun. 29 (2012) 87–91.
[35] X. Yu, Y. Huo, J. Yang, S. Chang, Y. Ma, W. Huang, Reduced graphene oxide supported Au nanoparticles as an efficient catalyst for aerobic oxidation of benzyl alcohol, Appl. Surf. Sci. 280 (2013) 450–455.
[36] M. Yang, Q. Ling, H. Yang, C. Li, A. Zhang, Enhanced catalytic activity of K-birnessite MnO 2 confined in carbon nanotubes for selective oxidation of benzyl alcohol, Catal. Commun. 46 (2014) 238–241.
[37] V.R. Choudhary, P.A. Chaudhari, V.S. Narkhede, Solvent-free liquid phase oxidation of benzyl alcohol to benzaldehyde by molecular oxygen using non-noble transition metal containing hydrotalcite-like solid catalysts, Catal. Commun. 4 (4) (2003) 171–175.
[38] Q. Tang, X. Gong, C. Wu, Y. Chen, A. Borgna, Y. Yang, Insights into the nature of alumina-supported MnOOH and its catalytic performance in the aerobic oxidation of benzyl alcohol, Catal. Commun. 10 (7) (2009) 1122–1126.
[39] J. Luo, F. Peng, H. Yu, H.J. Wang, Selective liquid phase oxidation of benzyl alcohol catalyzed by carbon nanotubes, Chem. Eng. J. 204 (2012) 98–106.
[40] S.F. Adil, M.E. Assal, M. Khan, A. Al-Warthan, M.R.H. Siddiqui, Nano silver-doped manganese oxide as catalyst for oxidation of benzyl alcohol and its derivatives: synthesis, characterisation, thermal study and evaluation of catalytic properties, Oxid. Commun. 36 (3) (2013) 778–791.
[41] H.B. Ji, T.T. Wang, M.Y. Zhang, Q.L. Chen, X.N. Gao, Green oxidation of alcohols by a reusable nickel catalyst in the presence of molecular oxygen, React. Kinet. Catal. Lett. 90 (2) (2007) 251–257.
[42] M. Yang, Q. Ling, R. Rao, H. Yang, Q. Zhang, H. Liu, A. Zhang, Mn 3 O 4-NiO-Ni/CNTs catalysts prepared by spontaneous redox at high temperature and their superior catalytic performance in selective oxidation of benzyl alcohol, J. Mol. Catal. A: Chem. 380 (2013) 61–69.
[43] S. Sultana, D. Kishore, M. Kuniyil, M. Khan, M.R.H. Siddiqui, A. Alwarthan, K. Prasad, N. Ahmad, S.F. Adil, Promoting effects of thoria on the nickel-manganese mixed oxide catalysts for the aerobic oxidation of benzyl alcohol, Arab. J Chem (2017).
[44] M.L. Kantam, R.S. Reddy, U. Pal, M. Sudhakar, A. Venugopal, K.J. Ratnam, F. Figueras, V.R. Chintareddy, Y. Nishina, Ruthenium/magnesium-lanthanum mixed oxide: An efficient reusable catalyst for oxidation of alcohols by using molecular oxygen, J. Mol. Catal. A: Chem. 359 (2012) 1–7.
[45] M.R.H. Siddiqui, I. Warad, S. Adil, R. Mahfouz, A. Al-Arifi, Nano-gold supported nickel manganese oxide: synthesis, characterisation and evaluation as oxidation catalyst, Oxid. Commun. 35 (2) (2012) 476.
[46] G. Wu, X. Wang, N. Guan, L. Li, Palladium on graphene as efficient catalyst for solvent-free aerobic oxidation of aromatic alcohols: Role of graphene support, Appl. Catal., B 136 (2013) 177–185.
[47] H. Wang, W. Fan, Y. He, J. Wang, J.N. Kondo, T. Tatsumi, Selective oxidation of alcohols to aldehydes/ketones over copper oxide-supported gold catalysts, J. Catal. 299 (2013) 10–19.
[48] C. Ragupathi, J.J. Vijaya, S. Narayanan, S. Jesudoss, L.J. Kennedy, Highly selective oxidation of benzyl alcohol to benzaldehyde with hydrogen peroxide by cobalt aluminate catalysis: a comparison of conventional and microwave methods, Ceram. Int. 41 (2) (2015) 2069–2080.
[49] T. Kawabata, Y. Shinozuka, Y. Ohishi, T. Shishido, K. Takaki, K. Takehira, Nickel containing Mg-Al hydrotalcite-type anionic clay catalyst for the oxidation of alcohols with molecular oxygen, J. Mol. Catal. A: Chem. 236 (1–2) (2005) 206–215.
[50] B.M. Choudary, M.L. Kantam, A. Rahman, C.V. Reddy, K.K. Rao, The first example of activation of molecular oxygen by nickel in Ni-Al hydrotalcite: a novel protocol for the selective oxidation of alcohols, Angew. Chem. Int. Ed. 40 (4) (2001) 763–766.
[51] G. Wu, Y. Gao, F. Ma, B. Zheng, L. Liu, H. Sun, W. Wu, Catalytic oxidation of benzyl alcohol over manganese oxide supported on MCM-41 zeolite, Chem. Eng. J. 271 (2015) 14–22.